



## Research paper

# Different distributions of calbindin and calretinin immunostaining across the medial and dorsal divisions of the mouse medial geniculate body

E. Lu<sup>a</sup>, D.A. Llano<sup>a,b,c,\*</sup>, S.M. Sherman<sup>a</sup><sup>a</sup> Department of Neurobiology, University of Chicago, USA<sup>b</sup> Department of Neurology, University of Chicago, USA<sup>c</sup> Abbott Laboratories, Abbott Park, IL, USA

## ARTICLE INFO

## Article history:

Received 20 June 2009

Received in revised form 23 July 2009

Accepted 23 July 2009

Available online 28 July 2009

## Keywords:

Thalamus

Cortex

Calcium

Intralaminar

Paralaminar

Auditory

## ABSTRACT

We studied the distributions of calretinin and calbindin immunoreactivity in subdivisions of the mouse medial geniculate body and the adjacent paralaminar nuclei. We found that the vast majority of labeled cells in the dorsal division of the medial geniculate body were immunoreactive for calbindin-only, whereas most of the remaining labeled cells were double-labeled. Very few calretinin+ only cells were observed. By contrast, we observed significant proportions of calbindin+ only, calretinin+ only and double-labeled cells in the medial division of the medial geniculate body. Further, the distributions of calbindin-only, calretinin-only and double-labeled cells did not differ between the medial division of the medial geniculate body, the supragenulate nucleus, the peripeduncular nucleus and the posterior intralaminar nucleus. We found essentially no somatic staining for either calbindin or calretinin in the ventral division of the medial geniculate body. These data suggest that there are distinct neurochemical differences between the two non-lemniscal auditory thalamic nuclei. In addition, these data extend previous observations that the medial division of the medial geniculate body shares many properties with the paralaminar group of nuclei.

© 2009 Elsevier B.V. All rights reserved.

## 1. Introduction

The presence or absence of several calcium-binding proteins, including calbindin (CB), parvalbumin (PV) and calretinin (CR), has been used to delineate different functional cell types in the neocortex, hippocampus, cerebellum and thalamus (Jones, 1998; Hof et al., 1999; Bastianelli, 2003; Jinno and Kosaka, 2006). The specific roles of these proteins in shaping neuronal activity have yet to be established, though it has been proposed that the differential total calcium-binding capacity and kinetics observed in these proteins can preferentially modulate specific types of calcium currents (Schwaller et al., 2002; Meuth et al., 2005).

Within the thalamus, the distribution of CB and PV are strikingly complementary, and these distributions have been used in the formulation of models of thalamic organization (Jones, 2001). For example, primary sensory thalamic nuclei (lateral geniculate nucleus, ventral posterior medial nucleus, ventral posterior lateral nu-

cleus and the ventral division of the medial geniculate body, MGBv) demonstrate immunostaining for PV, with label found in both somata and in the neuropil. CB staining in these regions is weak or non-existent. Non-primary sensory nuclei, such as the lateral posterior-pulvinar complex, posterior medial nucleus and the dorsal and medial subdivisions of the medial geniculate body (MGBd and MGBm, respectively) show strong somatic immunoreactivity for CB and poor to non-existent PV immunoreactivity (Rausell et al., 1992; de Venecia et al., 1995; Morel et al., 1997; Jones, 1998; Cruikshank et al., 2001). More recently, CR-immunoreactivity was demonstrated in the thalamus in several species, and was shown to generally have a similar distribution as CB in most thalamic nuclei (Arai et al., 1994; Fortin et al., 1998; Hof et al., 1999; FitzGibbon et al., 2000; Münkler et al., 2000; González et al., 2002), though CR positivity appears to be particularly prominent in the intralaminar and midline groups of nuclei (Arai et al., 1994; Oda et al., 2004; Uroz et al., 2004). Therefore, it appears that both CB and CR may be markers for the non-primary sensory thalamic nuclei.

This differential distribution of thalamic CB/CR and PV corresponds to differences in the presumed roles of these nuclei. For example, neurons in non-primary sensory thalamic nuclei receive large-terminal afferents, in part, from cortical layer 5 and have been referred to as “higher-order” nuclei (Sherman and Guillery, 2002). It has been proposed that higher-order thalamic nuclei

Abbreviations: CB, calbindin; CR, calretinin; PIN, posterior intralaminar nucleus; PP, peripeduncular nucleus; PV, parvalbumin; MGBd, dorsal division of the medial geniculate body; MGBm, medial division of the medial geniculate body; MGBv, ventral division of the medial geniculate body; PBS, phosphate-buffered saline; SG, supragenulate nucleus

\* Corresponding author. Address: Department of Neurobiology, University of Chicago, 549 E. 58th Street MC 0926, Chicago, IL 60637, USA. Tel.: +1 773 834 8764.

E-mail address: [a.daniel.llano@gmail.com](mailto:a.daniel.llano@gmail.com) (D.A. Llano).

receive receptive field information from one cortical area and relay it to another (Guillery, 1995). In contrast to the higher-order nuclei, primary sensory nuclei receive receptive field information from the sensory periphery and relay this information to the cortex, and have been referred to as “first-order” nuclei. For further discussion of first and higher-order thalamic nuclei, see (Sherman and Guillery, 2005). Thus, it appears that in the sensory thalamic nuclei, CB/CR and PV positivity may correspond to higher-order and first-order thalamic nuclei, respectively.

Though CR and CB have been observed in similar groups of higher-order nuclei, it is not known if CB and CR colocalize to the same population of neurons, or if separate populations of CB- and CR-positive neurons exist. The answer to this question has potentially important implications on our understanding of the organization of higher-order thalamic nuclei, since there is evidence for connectional and functional heterogeneity within higher-order thalamic nuclei. For example, many higher-order thalamic nuclei receive large-terminal afferents from both cortical and subcortical structures, raising the possibility that higher-order circuits, driven by cortical inputs, may reside in the same nuclei of first-order circuits, driven by subcortical inputs. In addition, though the prototypical projection of thalamic principal neurons is to layers 4 and 6 of neocortex, many thalamic cells in higher-order nuclei project to layer 1 of neocortex (Rockland et al., 1999) or to other subcortical structures, such as the basal ganglia or amygdala (Harting et al., 2001; Cheatwood et al., 2003). This projection pattern is particularly prevalent among neurons in the intralaminar and the adjacent “paralaminar” nuclei (Herkenham, 1980), such as the supragenulate (SG), posterior intralaminar nucleus (PIN) and the peripeduncular nucleus (PP, (Ryugo and Killackey, 1974; Ottersen and Ben-Ari, 1979; Clugnet et al., 1990)). The degree to which this heterogeneity may be reflected in different distributions of calcium-binding proteins has not yet been addressed.

In the current study, we take advantage of the tripartite organization of the auditory thalamus, which contains a PV-rich MGBv, and two CB/CR rich nuclei: the MGBd and MGBm. The MGBd receives large-terminal afferents from both the auditory cortex and external nuclei of the inferior colliculus and sends projections to layers 1, 4 and 6 of the secondary auditory cortical fields and layer 1 of the primary AC (Llano and Sherman, 2008). The MGBm receives input from the inferior colliculus, superior colliculus and spinal cord, and projects to layers 1 and 6 of cortex as well as to the basal ganglia and to the amygdala (Calford and Aitkin, 1983; Bordi and LeDoux, 1994; Linke, 1999). The MGBm also displays significant heterogeneity with respect to the intrinsic properties such that some neurons do not display bursting and there are subpopulations of neurons in the MGBm with large, reticular, non-bushy morphology (Winer and Morest, 1983; Smith et al., 2006). Given the functional and connectional heterogeneity in these nuclei, we hypothesized that distinct populations of CB-positive and CR-positive cells would be found in the MGBd and MGBm, and that the relative proportion of each cell type would differ.

## 2. Methods

### 2.1. Tissue processing

Adult (60-day or older) Balb/c mice of both sexes were used for this study. All surgical procedures were approved by the Institutional Animal Care and Use Committee at the University of Chicago, and animals were housed in animal care facilities approved by the American Association for Accreditation of Laboratory Animal Care (AAALAC). Every attempt was made to minimize the number of animals used and to reduce suffering at all stages of the study. Mice were sacrificed through deep anesthesia with ketamine hydrochloride

(100 mg/kg), and xylazine (3 mg/kg) and perfused transcardially with 4% paraformaldehyde in phosphate-buffered saline (PBS). The brains were postfixed overnight in perfusate. Brains were then cryoprotected in a series of increasing sucrose concentrations, up to 30% sucrose in PBS.

Frozen 30- $\mu$ m-thick sections were cut by using a sliding microtome. After being allowed to equilibrate in PBS (pH 7.4 in all instances) for at least 60 min, the sections were immersed in PBS containing 0.3% Triton-X to increase membrane permeability and prepare them for immunostaining. Sections were then blocked with 3% goat serum in 0.3% Triton-X for 30 min. Primary antibody solution consisted of a mix of 1:1000 CR (Swant rabbit anti-CR, code number 7699/4), and 1:1000 CB monoclonal antibodies (Sigma, product number C9848) in the goat serum solution. The anti-CR antibody was generated by immunizing rabbits with human calretinin. Specificity of this antibody has been established by the manufacturer, who has demonstrated the absence of binding in calretinin knock-out mice (<http://www.swant.com/pfd/Rabbit%20anti-calretinin%207699-4.pdf>). The anti-CB antibody was generated against purified bovine kidney calbindin D-28k. Per the manufacturer, this monoclonal antibody does not react with other members of the EF-hand family such as calbindin-D-9K, calretinin, myosin light chain, parvalbumin, S-100a, S-100b, S100A2 (S100L), or S100A6 (calyculin). Each lot was tested by using an immunoblot with bovine kidney cell extract as antigen and yields a single band at 28 kDa. For both anti-CR and anti-CB, we have run controls by eliminating the primary antibody and seen no signal.

Sections were incubated in the primary antibody solution overnight at room temperature. Afterwards, sections were washed three times using the Triton-X solution. Secondary antibody solution consisted of 1:200 goat biotinylated anti-rabbit antibody (Vector labs, BA-1000) for the CR-specific primary antibody and 1:100 Cy-2-conjugated anti-mouse antibody (AffiniPure Goat Anti-Mouse IgG conjugated to Cy-2, Jackson ImmunoResearch, catalog number 115-225-174) for the CB-specific primary antibody. The washed sections were incubated in the secondary antibody solution for 60 min at room temperature. After secondary antibody incubation, the sections were again washed three times in the Triton-X solution, and then incubated in a 1:100 streptavidin-alexafluor 594 conjugate (Invitrogen, catalog number S11227) solution for 60 min. Finally, the sections were washed thoroughly in PBS. All sections were mounted on gelatin-coated slides, air-dried, and coverslipped using anti-fade solution (Vectashield, Vector labs).

### 2.2. Imaging and analysis

All images were captured using a Retiga 2000R digital camera mounted to a Leica DM5000B microscope using a 100 W Mercury lamp with fluorescence optics. Leica TX2 filter cubes (Excitation 560 nm, Emission 645 nm, Dichroic 595 nm) were used to visualize calretinin signal and Leica L5 filter cubes (Excitation 480 nm, Emission 527 nm, Dichroic 505 nm) were used to visualize calbindin signal. Images were captured by using Q Capture Pro software. In direct imaging, the Capturer software was used to overlay the CR and CB images to create the double-labeled images.

NeuroLucida software (MBF Biosciences) was used for cell counting. For this, raw images were imported into NeuroLucida for analysis. The subdivisions of the thalamus were distinguished using Nissl-stains of the same sections used for immunostaining. For approximately 40% of sections, Nissl-stains were not available due to tissue damage during processing, and a mouse brain atlas (Paxinos and Franklin, 2008), was used for these sections. Borders were traced using NeuroLucida software, and for the MGBd, MGBm, SG and PP, cells within 25  $\mu$ m of any border were not counted to ensure that each cell could be unambiguously assigned to a particular nucleus. For PIN, which is a large structure with a large

number of cells, we only counted cells in a box,  $100 \times 100 \mu\text{m}$ , centered in the PIN. No analysis of subnuclei within the nuclei listed above was performed. Only “complete” cells (cells where the cell nucleus was visible) were counted, and double-labeled cells were marked manually using a separate symbol. Neurons were counted as positive if there was complete somatic cytoplasmic staining of the cell and there was substantial signal relative to background, as determined via visual inspection. Counting was performed on all complete immunoreactive neurons in the MGBd, MGBm, SG and PP. The actual number of cells marked was automatically tracked by NeuroLucida by symbol, and the cell counts reported were sums of the CR-only, CB-only and double-labeled cells. The symbols were color-coded afterwards for ease of reading the NeuroLucida cell maps.

The images were all imported into CorelDraw to adjust brightness/contrast and further tuning of color balance. No focal editing or focal changes in brightness or contrast were made.

### 2.3. Data analysis

We analyzed data from the MGBd, MGBm, SG, PIN and PP from two animals. In each animal, multiple sections from each MGB and adjacent nuclei were used for analysis. Data were pooled across the two animals and mean proportions of CB-only, CR-only or double-labeled cells in the three nuclei were compared using a  $\chi^2$ -test. Two  $\chi^2$ -tests were used: a  $3 \times 4$  contingency table was constructed to compare the distributions of immunoreactive neurons across the “paralamina” nuclei – MGBm, PIN, SG and PP and a  $3 \times 5$  contingency table was constructed that contained MGBm, PIN, SG, PP as well as the MGBd. To prevent false discovery, Bonferonni correction was used such that only p values less than 0.0125 were deemed significant. In addition, we compared the percentage of each cell type (CB-only, CR-only or double-labeled) in the anterior-most and posterior-most section of each side of each animal ( $n = 4$  sides total). Comparisons were made for each of the five

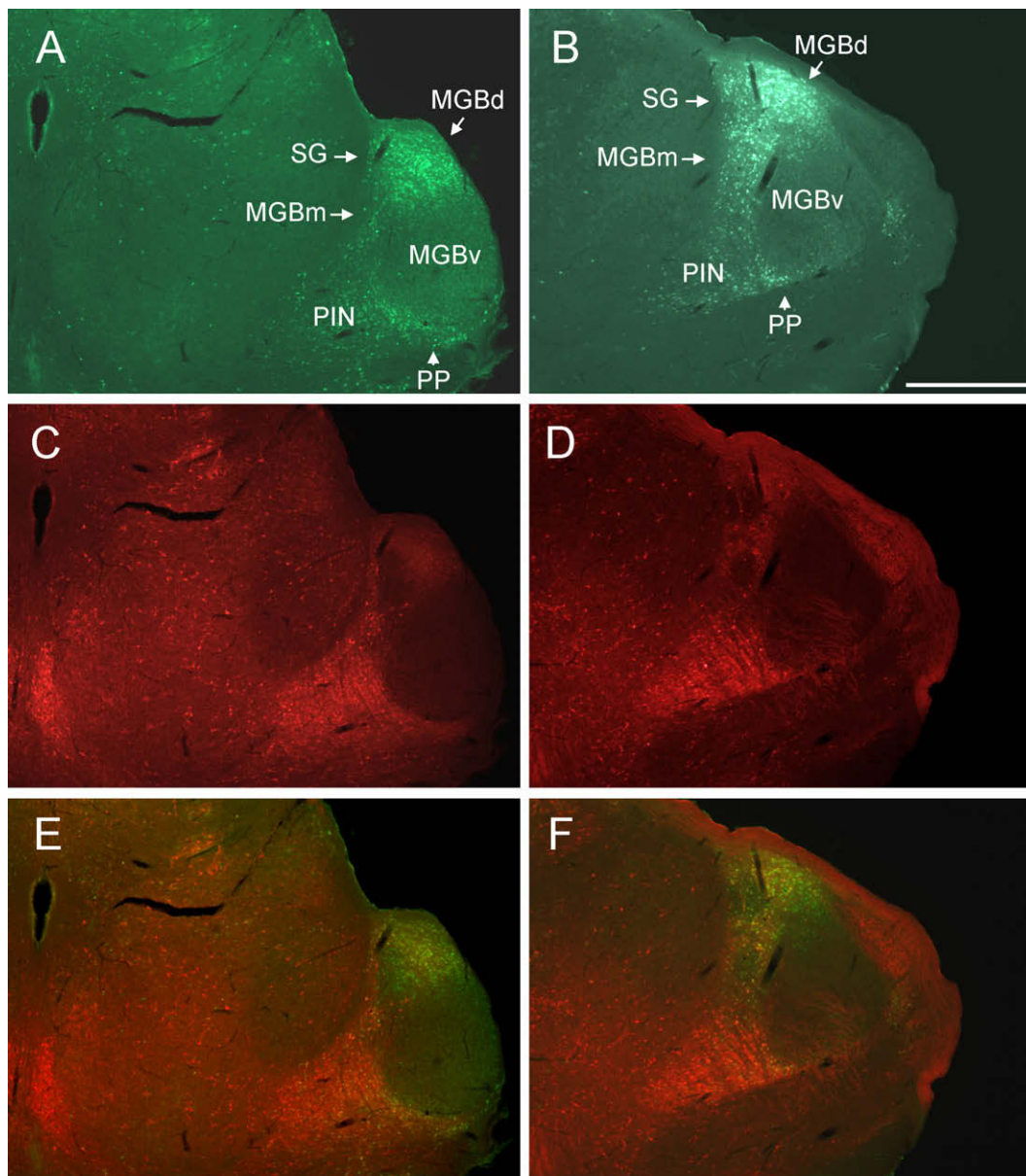


**Fig. 1.** Demonstration of distribution of CB-positive and CR-positive areas at two different rostro-caudal levels of the MGB. Left: bregma  $-3.28 \text{ mm}$ , Right: bregma  $-2.92 \text{ mm}$ . (A and B) Two sections from same mouse immunostained for CR, visualized with alexafluor 594. (C and D) Identical sections from A and B, immunostained for CB, visualized with Cy-2. (E) Overlay images from A and C. (F) Overlay images from B and D. Scale bar =  $500 \mu\text{m}$ . Images obtained using a Leica 5X/0.15 microscope objective.

subdivisions (MGBd, MGBm, PIN, SG and PP) using a Mann–Whitney *U*-test.

### 3. Results

Quantitative data were analyzed only from regions of the MGBd, MGBm, SG, PIN and PP in areas where subdivision labels can be unambiguously assigned. Thus, data from the rostral-most (rostral to  $-2.8$  mm from bregma) and caudal-most (caudal to  $-3.4$  mm from bregma) portions of the MGB were excluded.

Across the medial geniculate bodies of both mice, as described previously (Cruikshank et al., 2001), we observed prominent labeling for CB in all regions except the MGBv. Examples are shown at two rostro-caudal levels (bregma  $-3.28$  mm on left, bregma  $-2.92$  mm on right) in Fig. 1A and B). We found a similar general distribution of CR-positive cells across these subdivisions (see examples in Fig. 1C and D). Overlay images illustrating the distribution of CB- and CR-immunoreactivity are shown in Fig. 1E and F. We frequently observed double-labeled cells in the MGBm, SG, PIN and PP (see Fig. 2A–D), and found them less frequently in the MGBd. In general, CB-positive cells tended to have uniform somatic staining with essentially no neuropil staining. In contrast, CR

immunoreactivity was often noted throughout the cytoplasm, often leaving an unstained nucleus and demonstrating dense neuropil staining (see Fig. 2C).

We found differences in the distributions of CB+ only, CR+ only and double-labeled cells across the MGB subnuclei. Examples from two rostro-caudal levels (same sections as in Fig. 1) are shown in Fig. 3A–B. In the MGBd, we found essentially two cell types: CB+ only cells and double-labeled cells. In contrast, in the MGBm, SG, PIN and PP, we found significant numbers of all three cell types. The MGBv, as expected, had essentially no cells that were immunoreactive for either protein. The distributions of CB+ only, CR+ only and double-labeled cells across these subdivisions are shown across two animals in Fig. 4. In the MGBd, we observed that 1951 out of 2356 labeled neurons (83.3%) were CB+ only, with 347/2356 (14.3%) of neurons being positive for both proteins. A small number of neurons 58/2356 (2.4%) was CR+ only. By contrast, the three immunophenotypes were more evenly distributed in the MGBm, SG, PIN and PP. The distributions of the CB+, CR+ or double-label immunophenotypes across the MGBm (total  $n = 904$ ), SG ( $n = 387$ ), PIN ( $n = 1048$ ) and PP ( $n = 353$ ) were not significantly different ( $4 \times 3$  contingency table,  $\chi^2 = 3.14$ ,  $DF = 6$ ,  $p = 0.792$ ). Inclusion of the MGBd distributions into the  $\chi^2$ -analysis produced significant differences ( $5 \times 3$  contingency table,  $\chi^2 = 141$ ,  $DF = 8$ ,

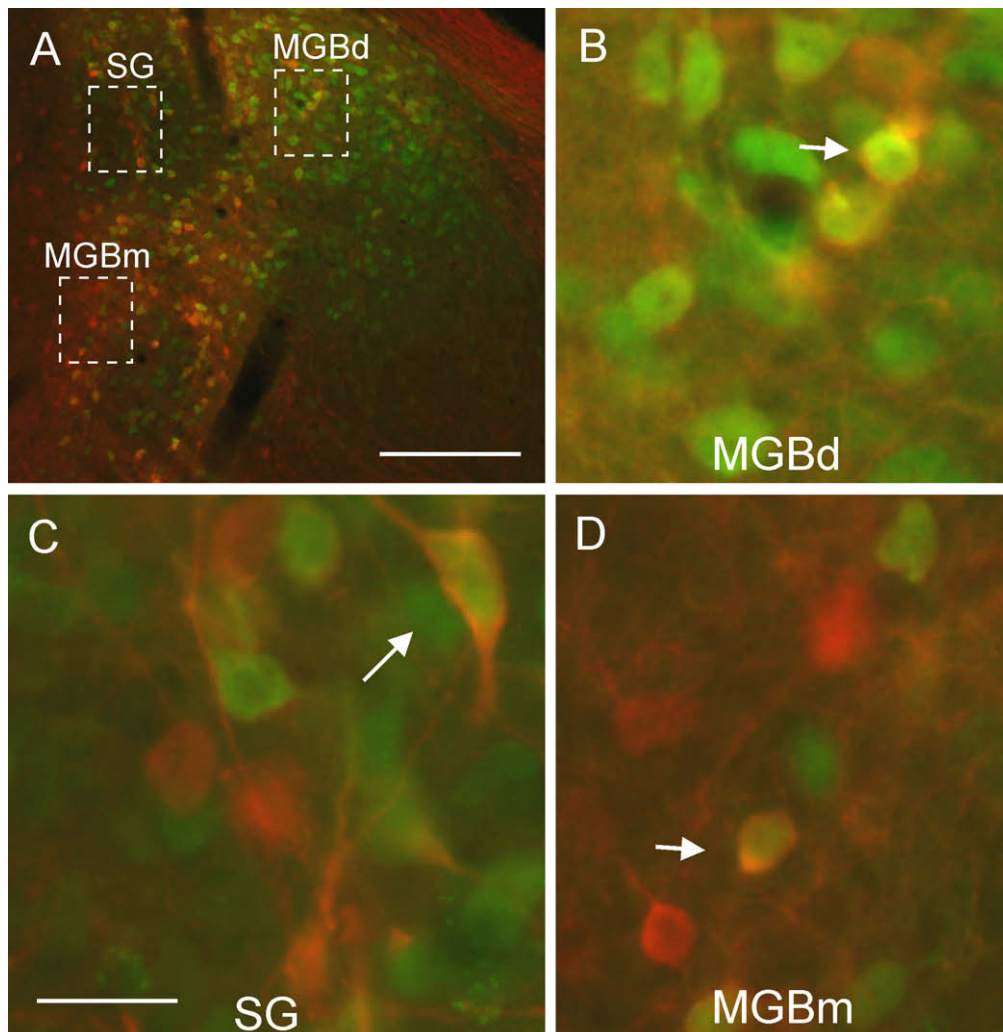


**Fig. 2.** Visualization of single- and double-labeled cells at  $10\times$  and  $20\times$ . (A)  $10\times$  image of section shown in right column of Fig. 1. Image obtained using a Leica N Plan  $10\times/0.25$  microscope objective. Scale bar =  $100\ \mu\text{m}$ . (B) Expanded view of dotted box in MGBd from Fig. 2A. Double-labeled cells are indicated by the white arrow. Scale bar =  $25\ \mu\text{m}$ . C and D are of the same scale as B. (C) Expanded view of the SG in the dotted white box. (D) Expanded view of the MGBm in the dotted white box. Images B–D obtained using a Leica  $20\times/0.5$  microscope objective.

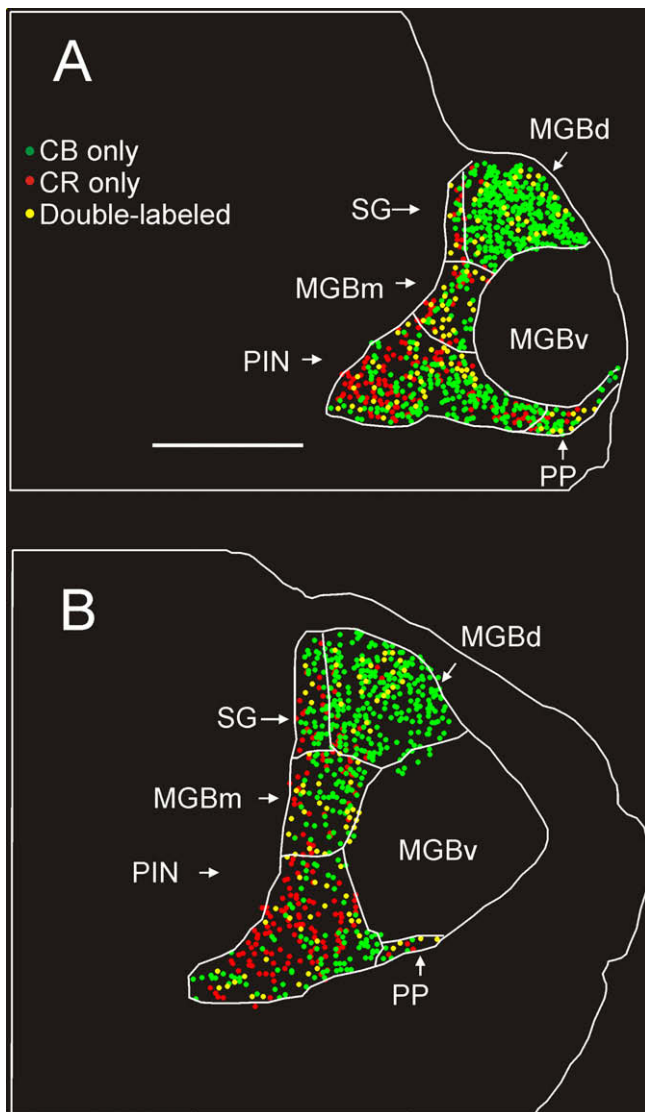


**Fig. 3.** (A and B) NeuroLucida plots of the distribution of CB-only (green), CR-only (red) and double-labeled cells (yellow) from the two images shown in Fig. 1. Only cells within the MGB complex, PIN, PP or SG are shown. Scale bar = 500  $\mu\text{m}$ .

$p < 0.001$ , for total numbers and percentages, see Table 1), indicating that the distribution of immunophenotypes in the MGBd differed from the distributions seen in the other four subdivisions. Similarly, when the distributions of immunophenotypes across each of the two animals were examined, no differences were seen across the MGBm, SG, PIN or PP (Mouse 1:  $\chi^2 = 10.9$ ,  $DF = 6$ ,  $p < 0.09$ , Mouse 2:  $\chi^2 = 6.35$ ,  $DF = 6$ ,  $p < 0.385$ ), but inclusion of the MGBd produced significant differences (Mouse 1:  $\chi^2 = 141$ ,  $DF = 8$ ,  $p < 0.001$ , Mouse 2:  $\chi^2 = 71.8$ ,  $DF = 8$ ,  $p < 0.001$ ).

In addition, we compared the percentages of CB+, CR+ or double-label cells in the anterior-most and posterior-most section of each side of each animal. A series of pairwise comparisons using a Mann–Whitney  $U$ -test across the five subdivisions did not reveal any significant differences (lowest  $p$  value = 0.3) in the percentage of immunophenotypes in any of the subdivisions.

#### 4. Discussion

In the current study, we demonstrate that the distribution of three potential immunophenotypes (CR+ only, CB+ only, double-la-

beled) differ substantially between the MGBd and the MGBm. Specifically, we found that the MGBd has mostly CB+ only neurons, a small number of double-labeled cells and very few CR+ only cells. In contrast, the MGBm has a substantial proportion of all three cell types. Furthermore, the distribution of immunophenotypes in the MGBm does not differ significantly from that seen in the adjacent paralaminae nuclei: the SG, PIN and PP. These data demonstrate that although the MGBd and MGBm have certain characteristics that would classify them as “higher-order” (significant CB-positivity, large-terminal corticothalamic afferents), they differ significantly in their distributions of CR, suggesting different roles for these two nuclei and extending previous observations that the MGBm contains many similarities with the paralaminae thalamic nuclei. Though these conclusions are drawn from two animals, all comparisons were made within the MGB complex and not from across animals, and the findings were highly consistent across both animals.

The only other study to our knowledge that examined the distribution of CB and CR double-labeled neurons in the thalamus is that of Leuba and Saini (1997), who immunostained human lateral inferior pulvinar and lateral geniculate nucleus for PV, CB and CR and found double-labeled thalamic cells to be quite scarce. There are several reasons why a larger percentage of double-labeled cells were observed in the current study. Here, the majority of double-labeled cells were found in the paralaminae nuclei, and the related MGBm, whereas, with the exception of the interlaminae layer of the lateral geniculate, the regions studied by Leuba and Saini (1997) are not considered to be part of the intralaminae or paralaminae system. In addition, Leuba and Saini (1997) utilized a non-fluorescent method (diaminobenzidine staining with or without metal intensification) for double-labeling, which greatly diminishes the sensitivity for identifying double-labeled cells.

The absence of a dominant immunophenotype in the MGBm compared to the MGBd is consistent with the comparatively greater heterogeneity in other domains described in the MGBm. Morphologically, Winer and Morest (1983) demonstrated multiple cell types in the cat MGBm, including radiate, tufted, elongated dendritic, small stellate and large, weakly tufted neurons. This variety is in contrast to the MGBd and MGBv, where radiate and tufted neurons dominate (Winer and Morest, 1983). Similarly, in the rat, Smith et al. (2006) found a variety of neuronal morphologies in the MGBm, such as neurons having long, sparsely branching dendritic trees, which were not observed in the MGBv or MGBd (Smith et al., 2006). Electrophysiologically, Smith et al. (2006) demonstrated that a substantial number of MGBm neurons do not demonstrate low-threshold bursting, which is found nearly uniformly in neurons in the MGBd and MGBv. In addition, whereas the primary targets of the MGBd are the secondary auditory cortical areas, the MGBm has major projections to the corpus striatum and the amygdala as well as targets throughout the primary and secondary auditory cortical areas (Ryugo and Killackey, 1974; Ottersen and Ben-Ari, 1979; Clugnet et al., 1990). It is not known if heterogeneity seen in immunophenotype distribution in the MGBm or PIN correspond to differential projection patterns to the amygdala or striatum. In this regard, it is worth noting that small injections of anterograde tracers into MGBm label both the amygdala and striatum, suggesting that any segregation in outputs may be more likely to be based by cellular features such as immunophenotype, rather than location within the MGBm (LeDoux et al., 1991).

Since CR+ only cells are virtually only seen in the MGBm, and not in other areas of the MGB, it is tempting to speculate that the unique properties seen in the MGBm, are restricted to CR+ only cells. A few investigators have studied immunophenotypes of upper layer-projecting thalamic neurons. Hashikawa et al. (1991) and Rubio-Garrido et al. (2007) placed retrograde tracer on the

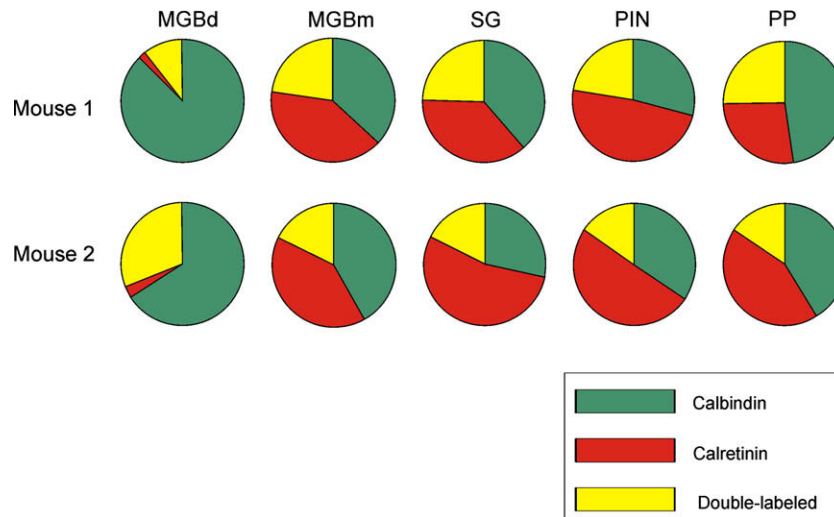


**Fig. 4.** Pie charts demonstrating the distribution of CB+ only, CR+ only and double-labeled cells across all three nuclei, shown for two different animals. The total number of cells counted for each nucleus is as follows: Mouse 1: MGBd (1839), MGBm (625), PIN (675), SG (224), PP (215), Mouse 2: MGBd (517), MGBm (279), PIN (373), SG (163), PP (138). In both mice, the distribution of immunophenotypes in the MGBd is significantly different from those in the MGBm, SG, PIN and PP (Mouse 1:  $\chi^2 = 141$ , DF = 8,  $p < 0.001$ , Mouse 2:  $\chi^2 = 71.8$ , DF = 8,  $p < 0.001$ ), whereas there was no difference in the distributions across the MGBm, SG, PIN and PP (Mouse 1:  $\chi^2 = 10.9$ , DF = 6,  $p < 0.09$ , Mouse 2:  $\chi^2 = 6.35$ , DF = 6,  $p < 0.385$ ).

surface of the monkey temporal lobe or rat cerebral hemisphere, respectively, and labeled the tissue with antibodies to CB and/or PV. Rubio-Garrido et al. (2007) found that although many retrogradely-labeled neurons also stained for CB, many more of the upper layer-projecting neurons were CB-negative, and most of the CB-positive cells were not back-labeled. Similarly, Hashikawa et al. (1991) found that although most backfilled neurons were CB+, at least 30% of them neurons were neither CB+ nor PV+. Neither study examined CR-immunoreactivity. In addition, in the primate lateral geniculate nucleus, CR positivity is only found in the S-layer (Soares et al., 2001), whereas CB is found in all interlaminar areas, and the S-layer is known to project to the upper layers of the visual cortex (Hendry and Yoshioka, 1994).

The similarity of the immunophenotype distributions between the MGBm and the paralamina thalamic nuclei adds to the mounting evidence that neurons in the MGBm share many properties of those in the paralamina nuclei, and/or those of the intralamina nuclei. Neurons in the intralamina nuclei across multiple species project outside of the middle cortical layers (often to layer 1), have significant numbers of non-bursting neurons, are less likely to have a typical bushy thalamocortical cell appearance and are more likely to be reticular (diffuse) in morphology, send major branches to the basal ganglia and many have been shown to stain prominently for CR and CB (with the exception of the centre median nucleus, which is PV-positive, Mönkle et al., 1999, 2000, Uroz et al., 2004, Morel et al., 1997, Fortin et al., 1998, Lacey et al., 2007, Beatty et al., 2009). As described above, all of these properties have been observed in MGBm neurons (Ryugo and Killackey, 1974; Ottersen and Ben-Ari, 1979; Winer and Morest, 1983; Clugnet et al., 1990; Smith et al., 2006). It has been proposed that the layer 1 inputs from the intralamina nuclei provide a timing-related signal or

play permissive role to facilitate maximal cortical activation in response to a thalamocortical signal from one of the non-intralamina nuclei (Llinas et al., 2002). Whether or not such a role may be extended to the paralamina nuclei, which would imply the presence of a modality-specific cortical activating system, has not yet been investigated.

An additional finding in the current study is the relative paucity of CR+ only cells in the MGBd, which has potential implications for use of calcium-binding proteins as potential markers of higher-order nuclei. In previous work, we have shown that the mouse MGBd receives large-terminal afferents from the primary auditory cortex, and have proposed that neurons that receive these afferents derive their receptive field information from the cortex, rather than the auditory midbrain (Llano and Sherman, 2008). Conflicting with this hypothesis is the presence of significant numbers of projections from the auditory midbrain to the MGBd, some of which contain large-terminal afferents (Bartlett et al., 2000). One potential resolution to this conflict is that higher-order and lower-order circuits may coexist within a nucleus, such that higher-order circuits consists of MGBd neurons driven by cortex, and lower-order circuits consist of MGBd neurons driven by the midbrain. As they have been used in classifying different pathways in the past, immunolabeling is a potential way of distinguishing these different circuits. Our immunolabeling study demonstrates that when one looks at calcium-binding proteins, there are at least two types of neurons in the MGBd: CB+, and double-labeled cells. It is not known whether a particular cell type receives driving input from cortex or midbrain, but one could potentially answer this question by examining the distribution of large-terminal synapses in a double- or triple-labeling study combining tracers of inputs to the MGBd with immunostaining for various calcium-binding proteins.

**Table 1**  
Distribution and percentages of CB+, CR+ and double-labeled cells, pooled across two animals.

	MGBd	MGBm	PIN	SG	PP
CB+	1951 (82.8%)	329 (36.4%)	336 (32.1%)	157 (40.6%)	158 (44.8%)
CR+	58 (2.5%)	379 (41.9%)	512 (48.9%)	155 (40.1%)	123 (34.8%)
Double-labeled	347 (14.7%)	196 (21.7%)	200 (19.1%)	75 (19.4%)	72 (20.4%)
Total labeled cells	2356	904	1048	387	353

Recent attempts to classify thalamic nuclei have proposed dichotomous schemes (First-order vs. Higher-order, Sherman and Guillery, 2005, or Core vs. Matrix, Jones, 2001) and in the system proposed by Jones (2001), calcium-binding protein immunoreactivity was explicitly used as part of this classification scheme. Though the current study did not examine parvalbumin staining in the MGB, we and others have demonstrated that parvalbumin staining is isolated to the MGBv (Cruikshank et al., 2001; Llano and Sherman, 2008). This, combined with the current study, suggests that there are at least four immunophenotypes (PV+ only, CB+ only, CR+ only and CB/CR double-labeled) differentially distributed across the MGB. Although the current study did not examine tissue stained for both PV and either CR or CB, previous studies have shown a virtual absence of PV staining outside of the MGBv (Cruikshank et al., 2001; Llano and Sherman, 2008), and the current study shows a virtual absence of CB or CR staining within the MGBv. Furthermore, CB/PV double-labeled cells have been observed very rarely in other areas of the thalamus (Jones and Hendry, 1989). We therefore assume that there are none or very few CB + PV or CR + PV double-labeled cells in the MGB. These data raise the possibility that neither of the two models presented above fully captures the diversity of thalamic nuclear types. The degree to which this heterogeneity in calcium-binding protein immunophenotype corresponds to other features non-homogeneously expressed in the thalamus, such as the post-synaptic target of thalamic neuron (cortex, striatum or amygdala), layer of cortical output, source of large-terminal input, presence of bursting etc., is currently unknown. Further, the functional significance of the presence or absence of PV, CB or CR remains to be elucidated. Answers to these questions may help further define the functional organization of the thalamus.

## Acknowledgements

The authors thank Angela Viaene for her technical assistance in the work. The authors obtained funding from the United States Public Health Service, NIH, Grants DC008320 (D.A.L.), EY03038 and DC008794 (S.M.S.).

## References

- Arai, R., Jacobowitz, D.M., Deura, S., 1994. Distribution of calretinin, calbindin-D28k, and parvalbumin in the rat thalamus. *Brain Research Bulletin* 33, 595–614.
- Bartlett, E.L., Stark, J.M., Guillery, R.W., Smith, P.H., 2000. Comparison of the fine structure of cortical and collicular terminals in the rat medial geniculate body. *Neuroscience* 100, 811–828.
- Bastianelli, E., 2003. Distribution of calcium-binding proteins in the cerebellum. *Cerebellum* 2, 242–262.
- Beatty, J.A., Sylwestrak, E.L., Cox, C.L., 2009. Two distinct populations of projection neurons in the rat lateral parafascicular thalamic nucleus and their cholinergic responsiveness. *Neuroscience* 162, 155–173.
- Bordi, F., LeDoux, J.E., 1994. Response properties of single units in areas of rat auditory thalamus that project to the amygdala. *Experimental Brain Research* 98, 275–286.
- Calford, M.B., Aitkin, L.M., 1983. Ascending projections to the medial geniculate body of the cat: evidence for multiple, parallel auditory pathways through thalamus. *Journal of Neuroscience* 3, 2365–2380.
- Cheatwood, J.L., Reep, R.L., Corwin, J.V., 2003. The associative striatum: cortical and thalamic projections to the dorsocentral striatum in rats. *Brain Research* 968, 1–14.
- Clugnet, M.C., LeDoux, J.E., Morrison, S.F., 1990. Unit responses evoked in the amygdala and striatum by electrical stimulation of the medial geniculate body. *Journal of Neuroscience* 10, 1055–1061.
- Cruikshank, S.J., Killackey, H.P., Metherate, R., 2001. Parvalbumin and calbindin are differentially distributed within primary and secondary subregions of the mouse auditory forebrain. *Neuroscience* 105, 553–569.
- de Venecia, R.K., Smelser, C.B., Lossman, S.D., McMullen, N.T., 1995. Complementary expression of parvalbumin and calbindin D-28k delineates subdivisions of the rabbit medial geniculate body. *The Journal of Comparative Neurology* 359, 595–612.
- FitzGibbon, T., Solomon, S.G., Goodchild, A.K., 2000. Distribution of calbindin, parvalbumin, and calretinin immunoreactivity in the reticular thalamic nucleus of the marmoset: evidence for a medial leaflet of incertal neurons. *Experimental Neurology* 164, 371–383.
- Fortin, M., Asselin, M.C., Gould, P.V., Parent, A., 1998. Calretinin-immunoreactive neurons in the human thalamus. *Neuroscience* 84, 537–548.
- González, G., Puelles, L., Medina, L., 2002. Organization of the mouse dorsal thalamus based on topology, calretinin immunostaining, and gene expression. *Brain Research Bulletin* 57, 439–442.
- Guillery, R.W., 1995. Anatomical evidence concerning the role of the thalamus in corticocortical communication: a brief review. *Journal of Anatomy* 187, 583–592.
- Harting, J.K., Updyke, B.V., Van Lieshout, D.P., 2001. Striatal projections from the cat visual thalamus. *European Journal of Neuroscience* 14, 893–896.
- Hashikawa, T., Rausell, E., Molinari, M., Jones, E.G., 1991. Parvalbumin- and calbindin-containing neurons in the monkey medial geniculate complex: differential distribution and cortical layer specific projections. *Brain Research* 544, 335–341.
- Hendry, S.H., Yoshioka, T., 1994. A neurochemically distinct third channel in the macaque dorsal lateral geniculate nucleus. *Science* 264, 575–577.
- Herkenham, M., 1980. Laminar organization of thalamic projections to the rat neocortex. *Science* 207, 532–535.
- Hof, P.R., Glezer, I.L., Condé, F., Flagg, R.A., Rubin, M.B., Nimchinsky, E.A., Vogt Weisenhorn, D.M., 1999. Cellular distribution of the calcium-binding proteins parvalbumin, calbindin, and calretinin in the neocortex of mammals: phylogenetic and developmental patterns. *Journal of Chemical Neuroanatomy* 16, 77–116.
- Jinno, S., Kosaka, T., 2006. Cellular architecture of the mouse hippocampus: a quantitative aspect of chemically defined GABAergic neurons with stereology. *Neuroscience Research* 56, 229–245.
- Jones, E.G., 1998. Viewpoint: the core and matrix of thalamic organization. *Neuroscience* 85, 331–345.
- Jones, E.G., 2001. The thalamic matrix and thalamocortical synchrony. *Trends in Neurosciences* 24, 595–601.
- Jones, E.G., Hendry, S.H., 1989. Differential calcium binding protein immunoreactivity distinguishes classes of relay neurons in monkey thalamic nuclei. *European Journal of Neuroscience* 1, 222–246.
- Lacey, C.J., Bolam, J.P., Magill, P.J., 2007. Novel and distinct operational principles of intralaminar thalamic neurons and their striatal projections. *Journal of Neuroscience* 27, 4374–4384.
- LeDoux, J.E., Farb, C.R., Romanski, L.M., 1991. Overlapping projections to the amygdala and striatum from auditory processing areas of the thalamus and cortex. *Neuroscience Letters* 134, 139–144.
- Leuba, G., Saini, K., 1997. Colocalization of parvalbumin, calretinin and calbindin D-28k in human cortical and subcortical visual structures. *Journal of Chemical Neuroanatomy* 13, 41–52.
- Linke, R., 1999. Differential projection patterns of superior and inferior collicular neurons onto posterior paralaminar nuclei of the thalamus surrounding the medial geniculate body in the rat. *European Journal of Neuroscience* 11, 187–203.
- Llano, D.A., Sherman, S.M., 2008. Evidence for nonreciprocal organization of the mouse auditory thalamocortical–corticothalamic projection systems. *The Journal of Comparative Neurology* 507, 1209–1227.
- Llinas, R.R., Leznik, E., Urbano, F.J., 2002. Temporal binding via cortical coincidence detection of specific and nonspecific thalamocortical inputs: a voltage-dependent dye-imaging study in mouse brain slices. *Proceedings of the National Academy of Sciences* 99, 449–454.
- Meuth, S.G., Kanyshkova, T., Landgraf, P., Pape, H.-C., Budde, T., 2005. Influence of Ca<sup>2+</sup>-binding proteins and the cytoskeleton on Ca<sup>2+</sup>-dependent inactivation of high-voltage activated Ca<sup>2+</sup> currents in thalamocortical relay neurons. *Pflügers Archiv European Journal of Physiology* 450, 111–122.
- Morel, A., Magnin, M., Jeanmonod, D., 1997. Multiarchitectonic and stereotactic atlas of the human thalamus. *The Journal of Comparative Neurology* 387, 588–630.
- Münkle, M.C., Waldvogel, H.J., Faull, R.L., 1999. Calcium-binding protein immunoreactivity delineates the intralaminar nuclei of the thalamus in the human brain. *Neuroscience* 90, 485–491.
- Münkle, M.C., Waldvogel, H.J., Faull, R.L.M., 2000. The distribution of calbindin, calretinin and parvalbumin immunoreactivity in the human thalamus. *Journal of Chemical Neuroanatomy* 19, 155–173.
- Oda, S., Kishi, K., Yang, J., Chen, S., Yokofujita, J., Igarashi, H., Tanihata, S., Kuroda, M., 2004. Thalamocortical projection from the ventral posteromedial nucleus sends its collaterals to layer I of the primary somatosensory cortex in rat. *Neuroscience Letters* 367, 394–398.
- Ottersen, O.P., Ben-Ari, Y., 1979. Afferent connections to the amygdaloid complex of the rat and cat. I. Projections from the thalamus. *The Journal of Comparative Neurology* 187, 401–424.
- Paxinos, G., Franklin, K.B.J., 2008. *The Mouse Brain in Stereotaxic Coordinates*, Compact 3rd Edition. The Coronal Plates and Diagrams, third ed. Academic Press.
- Rausell, E., Bae, C.S., Vinuela, A., Huntley, G.W., Jones, E.G., 1992. Calbindin and parvalbumin cells in monkey VPL thalamic nucleus: distribution, laminar cortical projections, and relations to spinothalamic terminations. *Journal of Neuroscience* 12, 4088–4111.
- Rockland, K.S., Andresen, J., Cowie, R.J., Robinson, D.L., 1999. Single axon analysis of pulvinocortical connections to several visual areas in the Macaque. *The Journal of Comparative Neurology* 406, 221–250.

- Rubio-Garrido, P., Pérez-de-Manzo, F., Clascá, F., 2007. Calcium-binding proteins as markers of layer-I projecting vs. deep layer-projecting thalamocortical neurons: A double-labeling analysis in the rat. *Neuroscience* 149, 242–250.
- Ryugo, D.K., Killackey, H.P., 1974. Differential telencephalic projections of the medial and ventral divisions of the medial geniculate body of the rat. *Brain Research* 82, 173–177.
- Schwaller, B., Meyer, M., Schiffmann, S., 2002. 'New' functions for 'old' proteins: The role of the calcium-binding proteins calbindin D-28k, calretinin and parvalbumin, in cerebellar physiology. Studies with knockout mice. *Cerebellum* 1, 241–258.
- Sherman, S.M., Guillery, R.W., 2002. The role of the thalamus in the flow of information to the cortex. *Philosophical Transactions of the Royal Society B: Biological Sciences* 357, 1695–1708.
- Sherman, S.M., Guillery, R.W., 2005. *Exploring the Thalamus and its Role in Cortical Function*. The MIT Press.
- Smith, P.H., Bartlett, E.L., Kowalkowski, A., 2006. Unique combination of anatomy and physiology in cells of the rat paralaminar thalamic nuclei adjacent to the medial geniculate body. *The Journal of Comparative Neurology* 496, 314–334.
- Soares, J.G.M., Botelho, E.P., Gattass, R., 2001. Distribution of calbindin, parvalbumin and calretinin in the lateral geniculate nucleus and superior colliculus in *Cebus apella* monkeys. *Journal of Chemical Neuroanatomy* 22, 139–146.
- Uroz, V., Prensa, L., Giménez-Amaya, J.M., 2004. Chemical anatomy of the human paraventricular thalamic nucleus. *Synapse* 51, 173–185.
- Winer, J.A., Morest, D.K., 1983. The medial division of the medial geniculate body of the cat: implications for thalamic organization. *Journal of Neuroscience* 3, 2629–2651.